SEISMIC DESIGN GROUND MOTIONS FOR STRAIT-CROSSING PROJECTS IN JAPAN

by

Masahiko Yasuda[1], Keiichi Tamura[2], Shojiro Kataoka[3] and Yoshihiro Nakao[3]

ABSTRACT

In order to establish rational seismic design for strait-crossing projects in Japan, it is most essential to appropriately consider the effects of near field ground motions of large earthquakes. For this purpose, we study the applicability of semi-empirical and stochastic Green's function techniques to estimate near field ground motions, by synthesizing ground motion for the large-scale scenario earthquakes, in which earthquake source parameters are systematically changed. Based on the results of analysis, variation of ground motion resulting from uncertainty of source parameters is discussed.

Key words: strait-crossing project, seismic design, ground motion, Green's function, earthquake source parameter

INTRODUCTION

Feasibility of super long-span bridges crossing straits is being studied in Japan to meet the goal of constructing a multi-nuclei nation as set forth in the Comprehensive National Development Plan (National Land Agency, 1998). Some of these bridges will be located over or nearby the fault planes of past large earthquakes. For instance, the 1923 Kanto Earthquake (M_J=7.9, M_J is the Japan Meteorological Agency Magnitude) and 1944 Tonankai Earthquake (M_J=7.9) occurred in Tokyo Bay and Ise Bay regions, respectively, and two highway routes are being planned to cross the mouths of these two bays.

For establishing seismic design ground motions of large structures, seismic risk analysis and attenuation relation of ground motion have been widely used in Japan including the Trans-Tokyo Bay Highway Bridge (Public Works Research Institute, 1991) and Akashi Kaikyo Bridge (Honshu-Shikoku Bridge Authority, 1988). In the seismic risk analysis, an attenuation equation is usually incorporated to estimate ground motion intensity from an expected earthquake magnitude and distance. Although an attenuation equation is a simple and effective tool of engineering practice to predict ground motion, it should be noted that the applicability of this technique to the near field of large earthquake is limited, because it is an empirical formula and does not usually contain strong motion data obtained in the near fields of large earthquakes. Appling attenuation relation to the near field by substituting small value for distance may yield excessive ground motion for seismic design of structures.

The semi-empirical ground motion synthesizing method (e.g., Hartzell, 1978; Irikura, 1983), in which ground motion record from a small event is used as Green's function, has recently been applied to earthquake engineering. This technique can incorporate complicated earthquake source mechanism into calculation,

1) Formerly, Director, Earthquake Disaster Prevention Research Center, Public Works Research Institute, Ministry of Construction, Tsukuba-shi, Ibaraki-ken 305-0804 Japan
2) Head, Ground Vibration Division, ditto
3) Research Engineer, Ground Vibration Division, ditto

and has an advantage of estimating near field motions. On the other hand, this method requires various source parameters, and most of them are difficult to be determined accurately, especially for a future earthquake.

In addition to those facts, the semi-empirical method requires an actual small event record, however, it is obvious that an appropriate record is not always available. To make up this disadvantage, stochastic synthetic method has been proposed (e.g., Kamae, et al., 1991), in which stochastically simulated small event motion is used as a Green's function.

To establish rational seismic design ground motions for strait-crossing projects, we are studying the applicability of semi-empirical and stochastic Green's function techniques at the Public Works Research Institute. In this paper we simulate ground motion at Tokyo Bay region, assuming the Kanto Earthquake, which will be most influential over this area. We employ geometric parameters of the 1923 Kanto Earthquake and change dynamic source parameters variously, and examine influence of uncertainty of source parameters on the synthesized ground motion, as a basis of developing design ground motions for strait-crossing projects.

GROUND MOTION SIMULATION USING SEMI-EMPIRICAL GREEN'S FUNCTION TECHNIQUE

To simulate ground motions from a large event, ground motion record from a small event such as foreshock or aftershock that occurred within the fault area of large event is used as Green's function. The fault plane of the target event is divided into sub-faults so that their sizes coincide with the fault area of small event. The Green's functions are superimposed considering time delay due to fault rupture from the hypocenter to a sub-fault and wave traveling from each sub-fault to the estimation point. An advantage of using small event record as Green's function exists in that complicated path and site effects are incorporated automatically into ground motion estimation, which has large influence over the accuracy of simulating short period ground motions.

Temporal and spatial variations of dislocation are considered here by introducing $T_{mn}(\omega)$ and ω_{mn}, respectively, and the Fourier transform of displacement from a large event $u(\omega)$ is expressed as:

$$u(\omega)=\sum_{m=1}^{N}\sum_{n=1}^{N} T_{mn}(\omega)\omega_{mn}u_0(\omega)\exp(-i\omega\tau_{mn}) \tag{1}$$

where,

T_{mn} : Function representing the difference in source time function between small and large events (Irikura, 1986)

$$T_{mn}(\omega)=1+(N-1)\frac{\dfrac{\sin\dfrac{\omega\tau}{2}}{\dfrac{\omega\tau}{2}}}{\dfrac{\sin\dfrac{\omega\tau}{2(N-1)N_1}}{\dfrac{\omega\tau}{2(N-1)N_1}}}\cdot\exp\left[-i\left(\frac{\omega\tau}{2}-\frac{\omega\tau}{2(N-1)N_1}\right)\right] \tag{2}$$

ω_{mn} : Weight function representing spatial variation of dislocation

u_0 : Frequency component of ground motion from small event

τ_{mn} : Time delay due to fault rupture from hypocenter to sub-fault and wave

traveling from sub-fault to estimation point.

N : Number of sub-faults

τ : Rise time

N_1 : Coefficient to avoid the synthetically generated periodicity

The source time function after Irikura (1986) is used in the present study, which is shown in Figure 1.

VARIATION OF EARTHQUAKE SOURCE PARAMETERS

Target Event and Basic Source Parameters

We employ a source model of the 1923 Kanto Earthquake proposed by Wald and Somerville (1995). The major parameters of this model are listed in Table 1. Ground motion at Kannonzaki is synthesized in this study. We use a strong motion data from the 1987 Chiba-ken Toho-oki Earthquake (M_J=6.7) as a small event record, which was obtained on the siltstone at Kannonzaki. The fault plane of 1923 Kanto Earthquake, and locations of epicenters of the Kanto and Chiba-ken Toho-oki Earthquakes and Kannonzaki are presented in Figure 2. Figures 3 and 4 show acceleration waveform and acceleration response spectrum (damping ratio h=0.05) of Kannonzaki record, respectively.

Since the seismic moment of the Chiba-ken Toho-oki Earthquake is calculated as 7.05×10^{25} [dyne-cm] after Harvard University (1999), the fault plane of Kanto Earthquake is divided into 5×5 sub-faults in the following analysis, according to the seismic moment ratio between two earthquakes.

Source Parameters Changed

We systematically change fault rupture mode and location of asperity to examine their influence on the synthesized ground motion (Tamura et al., 1999). We assume lateral rupture and radial rupture as illustrated in Figure 5, i.e., 5 cases for lateral rupture and 15 cases for radial rupture. According to Somerville et al. (1999), the area of asperity that has twice as large as average slip is 22% of total fault plane area, and we assign asperity for 6 sub-faults out of 25 sub-faults. Note that their result was derived from analysis of 15 crustal earthquakes, and further study may be necessary to apply it directly to the inter-plate Kanto Earthquake. We employ 2×3 and 3×2 asperities as shown in Figure 6. For each asperity shape, we assume 9 patterns of asperity distribution. Consequently, we set up (5+15)×(9+9)=360 cases for numerical simulation at this stage.

In addition to the above-mentioned asperity models, we also employ the variable-slip rupture model of the 1923 Kanto Earthquake proposed by Wald and Somerville (1995) for reference. Note that the slip vector is determined for each sub-fault in this model, however we use the slip amplitude and ignore slip angle in the present study. When we use this model, we assume bilateral rupture from the hypocenter that is indicated by a star in Figure 7, and other source parameters are set as the same as shown in Table 1.

Since the ground motion estimation point (Kannonzaki) is located over almost the center of fault plane as shown in Figure 2, some of assumed simulation cases yield similar results when symmetric rupture mode and location of asperity is assigned. Besides this, in the previous study (Tamura et al., 1999), we confirmed that the horizontal location of 2×3 asperity and vertical location of 3×2 asperity do not affect much calculation result, respectively. Considering those facts, we reassign rupture

mode and asperity locations as indicated in Figures 8 and 9. Then, numerical simulation cases are reduced to 124 cases (Table 2).

VARIATION OF GROUND MOTION DUE TO UNCERTAINTY OF SOURCE PARAMETERS

Acceleration response spectra of the 124 cases are overlaid in Figure 10, where damping ratio is taken as h=0.05. Variation of spectral amplitude depends on natural period, and it ranges from 3 to 6 times. We should be attentive that this variation is inevitable when we infer ground motion for a future earthquake that has uncertain source parameters. Figure 11 shows acceleration response spectrum using the variable-slip rupture model that is shown in Figure 7. Comparing those two figures, result from the variable-slip rupture model gives almost upper bound of variation of synthesized ground motion.

GROUND MOTION SIMULATION USING STOCHASTIC GREEN'S FUNCTION TECHNIQUE

Procedure of Ground Motion Simulation

Here, the ground motion due to each sub-fault is simulated stochastically and employed as a Green's function to synthesize ground motion of a large event. The ground motions on the seismic bedrock at Kannonzaki generated from sub-faults are produced to match observed ground motions in a stochastic sense and superimposed considering time delay due to the fault rupture process and the wave propagation. The superimposed motion multiplied by the transfer function of the ground structure between the ground surface and the seismic bedrock makes the synthetic motion on the ground surface at Kannonzaki. Table 3 and Figure 12 show the ground structure model and the transfer function at Kannonzaki used in the following simulation.

Boore (1983) modeled the acceleration spectrum $A(f)$ of shear waves at a site of which distance R from a source with seismic moment M_0 as:

$$A(f) = \frac{F}{4\pi\rho\beta^3} M_0 \cdot \frac{(2\pi f)^2}{1+(f/f_c)^2} \cdot \frac{1}{\sqrt{1+(f/f_{max})^s}} \cdot \frac{1}{R} \exp\left(-\frac{\pi f R}{Q(f)\beta}\right) \cdot \sqrt{\frac{\rho\beta}{\rho_b\beta_b}} \quad (3)$$

where,

- F : Radiation pattern coefficient
- ρ : Density at the source fault
- β : Shear velocity at the source fault
- f_c : Corner frequency
- f_{max} : Cut-off frequency
- s : Decay rate at high frequencies
- $Q(f)$: Quality factor
- ρ_b : Density at the site
- β_b : Shear velocity at the site

Equation (3) was formed following the theories of source spectrum and the parameters f_c, f_{max}, and s are chosen to match ground motion records. The last term of the right-hand side of Equation (3) is added to consider the amplification due to the ground structure between the source and the site (Dan et al., 2000).

We employ the shaping window by Jennings et al. (1968) to obtain the phase spectrum and generate a transient accelerogram whose amplitude spectrum matches Equation (3). The shaping window consists of three parts: amplifying part (quadratic curve), strong motion part (constant), and attenuating part (exponential curve) as shown in Figure 13.

VARIATION OF GROUND MOTION DUE TO UNCERTAINTY OF SOURCE PARAMETERS

The effects of the locations of hypocenter and asperities on the simulated ground motions are examined by changing them systematically on the fault plane.

Variation of Ground Motion due to Location of Hypocenter

The ground motions are simulated using 15 locations of hypocenter shown as solid circles in Figure 14. The slip of each sub-fault is assigned following the variable-slip model of the 1923 Kanto Earthquake (Wald and Somerville, 1995) shown in Figure 7.

Figure 15 shows the acceleration response spectra (h=0.05) of the simulated ground motions. We see the acceleration response varies about 3 times due to the location of hypocenter and the variation in long natural period range is somewhat larger than in short period range. The result from the simulation in which the location of hypocenter of the 1923 Kanto Earthquake shows the acceleration response close to the upper bound of the variation in short period range and mean of the variation in long period range.

Identification and Simplification of Asperities

Somerville et al. (1999) proposed a procedure to identify rectangle asperities from a variable-slip model and applied it to 15 crustal earthquakes. Figure 15 shows the rectangle asperities identified from the variable-slip model of the 1923 Kanto Earthquake by the procedure. Since two asperities were identified here, we call the larger one "Asp#1" and the smaller "Asp#2". The average slip over Asp#1 and Asp#2 become 2.00 times and 2.09 times of the average slip over the entire fault, i.e., 2.40[m]. Those values are very close to the value, 2.01, which Somerville et al. (1999) found as the average of the 15 crustal earthquakes.

Therefore, we simplify Asp#1 and Asp#2 to have uniform slip 4.80[m], just 2 times of the average slip over the entire fault. The rest of the entire fault is set to have uniform slip 1.57[m] to maintain the average slip over the entire fault. Here we call the simplified slip model "rectangle asperity model".

Figure 16 compares the simulated ground motions and their acceleration response spectra due to the rectangle asperity and variable-slip models. The location of hypocenter of the 1923 Kanto Earthquake is used here. Since the results show a fairly good agreement, we can use the rectangle asperity model and change the locations of Asp#1 and Asp#2 to examine the effects of variation of the slip distribution on the ground motion.

Variation of Ground Motion due to Location of Asperities

According to the result of a preliminary analysis, it was found that the effects of changing the location of Asp#1 in the dip direction on the ground motion are negligible. Thus, as shown in Figure 17, the locations of Asp#1 and Asp#2 are changed systematically with the location of Asp#1 in the dip direction is fixed. The location of hypocenter of the 1923 Kanto Earthquake is used here.

Figure 18 compares the acceleration response spectra (h=0.05) from the 18 rectangle asperity models shown in Figure 17. Figure 18 also shows the acceleration response spectrum from the variable-slip model of the 1923 Kanto

Earthquake, which is almost upper bound of the variation of the other 18 cases. This means the sub-faults that have large slips were concentrated around Kannonzaki as we can see in Figure 14. We see the acceleration response varies about 3 times and the variation in short period range is somewhat larger than in long period range, which is inverse of the effects of the location of hypocenter.

CONCLUSIONS

Ground motion at the mouth of Tokyo Bay from the large-scale scenario earthquakes were synthesized by semi-empirical and stochastic Green's function techniques. The geometric source parameters of the 1923 Kanto Earthquake were incorporated into the simulation, while the dynamic parameters, such as fault rupture mode, locations of hypocenter and asperities were systematically changed to study their influence on the synthesized ground motion. The following conclusions may be deduced from the present study.

1) The peak amplitude of 5% damped acceleration response spectrum calculated from the synthesized ground motion for the Kanto Earthquake is generally about 3000 cm/s^2.

2) Variation of fault rupture mode and asperity affects synthesized ground motion over wide period range, and the spectral amplitude of resultant ground motion synthesized by the semi-empirical Green's function technique changes 3 to 6 times due to this variation.

3) Acceleration response spectrum estimated by the stochastic Green's function technique also varies about 3 times over the natural period range under consideration.

4) The variable-slip rupture model yields almost upper bound of synthesized ground motions within the scope of present study. This is attributed to a fact that the sub-faults with large slips were concentrated beneath the ground motion estimation point.

REFERENCES

Boore, D. M. (1983). "Stochastic Simulation of High-frequency Ground Motions based on Seismological Models of the Radiated Spectra", *Bulletin of Seismological Society of America*, Vol.73, No.6.

Dan, K. et al. (2000). "Isoseismal Map of Strong Motions for the 1923 Kanto Earthquake (M_{JMA} 7.9) by Stochastic Green's Function Method", *Journal of Structural and Construction Engineering*, Architectural Institute of Japan (in Japanese, Submitting).

Hartzell, S. (1978). "Earthquake Aftershocks as Green's Functions", *Geophysical Research Letters*, Vol.5, No.1.

Harvard University (1999). *The Harvard CMT Catalog*.

Honshu-Shikoku Bridge Authority (1988). *Seismic Design Guideline of Akashi Kaikyo Bridge (Draft)* (in Japanese).

Irikura, K. (1983). "Semi-Empirical Estimation of Strong Ground Motions during Large Earthquakes", *Bulletin of Disaster Prevention Research Institute*, Kyoto University, Vol.33, No.298.

Irikura, K. (1986). "Prediction of Strong Acceleration Motions Using Empirical Green's Function", *Proc. of 7th Japan Earthquake Engineering Symposium*.

Jennings, P. C. et al. (1968). "Simulated Earthquake Motions", *Report of Earthquake Engineering Research Laboratory*, California Institute of Technology.

Kamae, K. et al. (1991). "Prediction of Strong Ground Motion Based on Scaling Law of

Earthquakes by Stochastic Synthesis Method", *Journal of Structural and Construction Engineering*, Architectural Institute of Japan, No.430 (in Japanese).

National Land Agency (1998). *The Grand Design for National Development in the 21st Century* (in Japanese).

Public Works Research Institute (1991). "Study on Structural Design of Trans-Tokyo Bay Highway", *Report of PWRI*, Vol.184 (in Japanese).

Somerville, P. et al. (1999). "Characterizing Crustal Earthquake Slip Models for the Prediction of Strong Ground Motion", *Seismological Research Letters*, Vol.70, No.1.

Tamura, K. et al. (1999). "Developing Seismic Design Ground Motions for Super Long-span Bridges", *Proc. of 15th U.S.-Japan Bridge Engineering Workshop*, U.S.-Japan Panel on Wind and Seismic Effects, UJNR.

Wald, D. and Somerville, P. (1995). "Variable-Slip Model of the Great 1923 Kanto, Japan Earthquake: Geodetic and Body-Waveform Analysis", *Bulletin of Seismological Society of America*, Vol.85, No.1.

Table 1 Source Parameters of the 1923 Kanto Earthquake

Fault Length	130 [km]
Fault Width	70 [km]
Strike	290 [deg]
Dip	25 [deg]
Seismic Moment	7.8×10^{27} [dyne·cm]
Rupture Velocity	3.0 [km/s]
Rise Time	5 [s]

Table 2 Number of Reassigned Simulation Cases

Rupture starts from the center	(1+3) ×(3+4)=28 cases
Rupture does not start from the center	(2+6) ×(6+6)=96 cases
Total	124 cases

Table 3 Ground Structure Model at Kannonzaki

	Depth [m]	Density [t/m^3]	S Wave Velocity [km/s]
ground surface	0 ~ 31	1.9	0.42
	31 ~ 45	1.9	0.40
	45 ~ 57	1.9	0.50
	57 ~ 77	1.9	0.61
	77 ~ 94	1.9	0.70
	94 ~ 120	1.9	0.84
	120 ~ 1005	2.0	1.15
	1005 ~ 1405	2.0	1.20
	1405 ~ 2605	2.1	1.30
	2605 ~ 3005	2.3	1.40
seismic bedrock	3005 ~	2.5	2.72

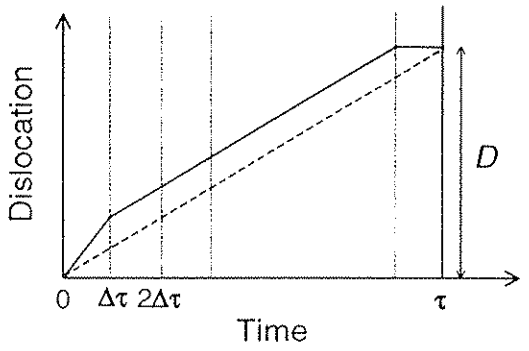

Figure 1 Source Time Function (Irikura, 1986)

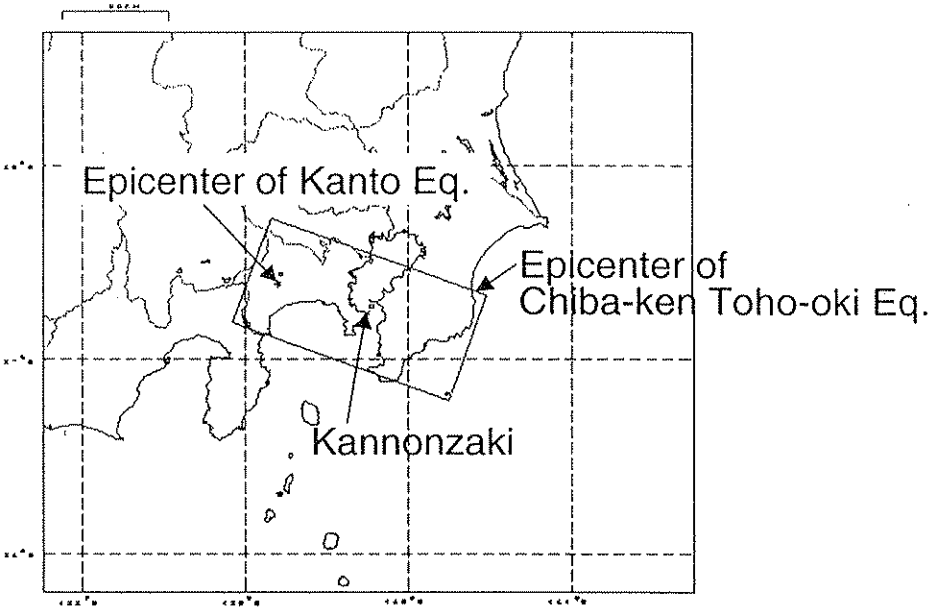

Figure 2 Fault Plane, and Locations of Epicenters and Kannonzaki

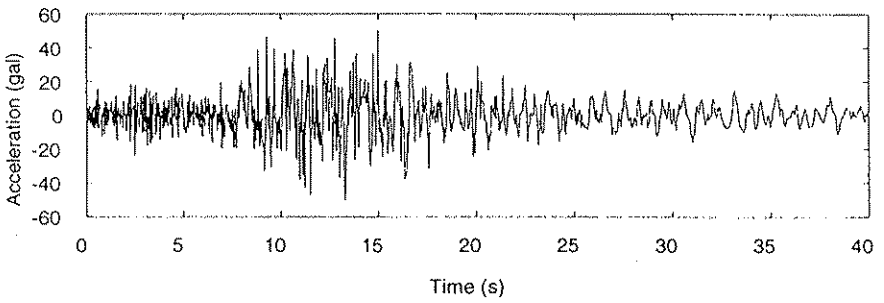

Figure 3 Kannonzaki Record from the 1987 Chiba-ken Toho-oki Earthquake (N-S Component)

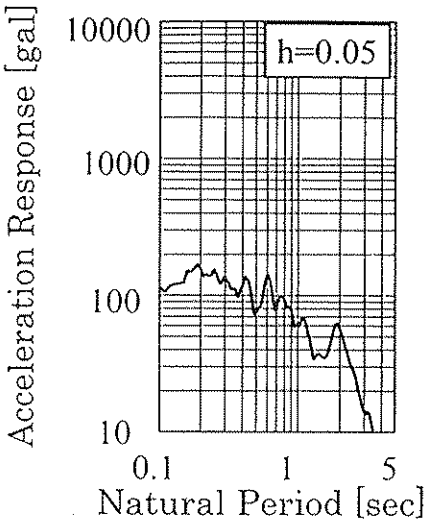

Figure 4 Acceleration Response Spectrum of Kannonzaki Record (h=0.05)

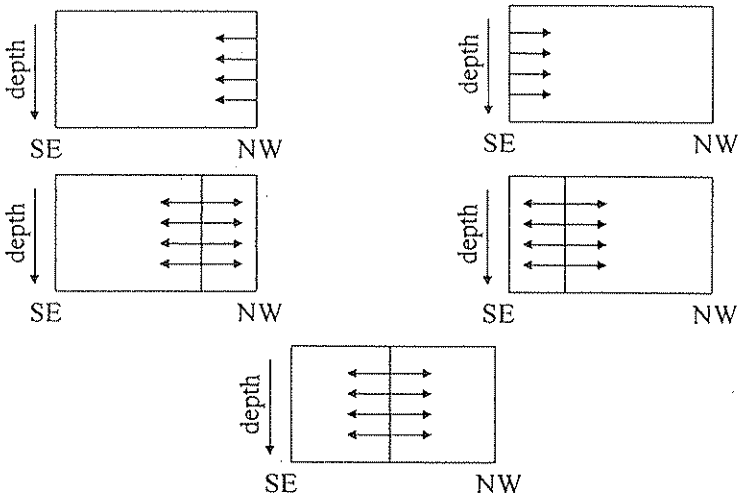

(a) Unilateral and Bilateral Rupture

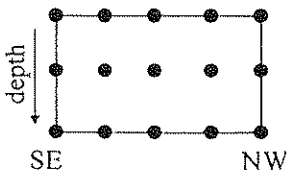

(b) Hypocenters of Radial Rupture

Figure 5 Rupture Modes and Hypocenters of Radial Rupture

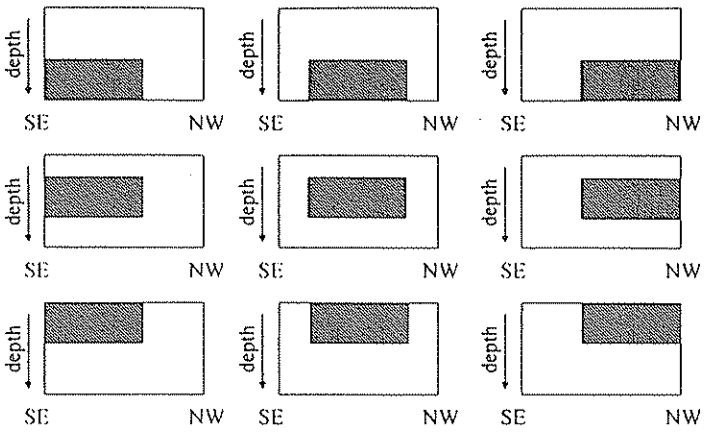

(a) 2×3 Asperity

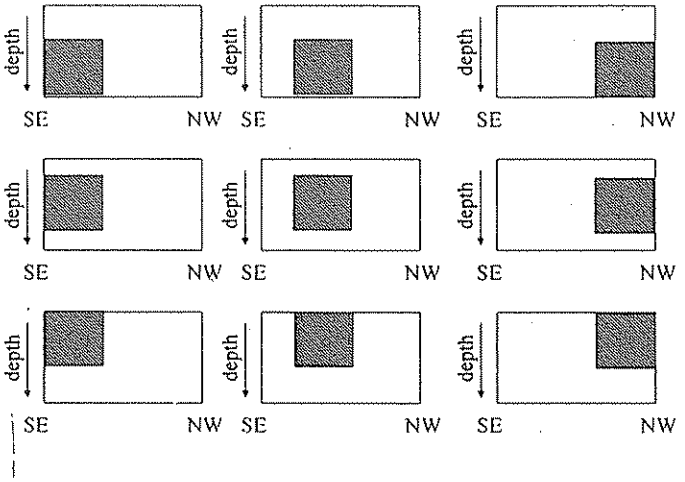

(b) 3×2 Asperity

Figure 6 Asperity Shape and Locations

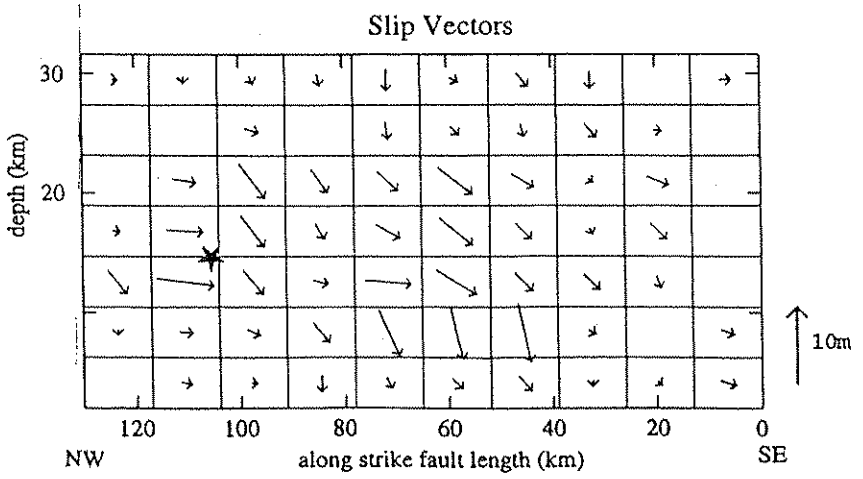

Figure 7 Variable-Slip Rupture Model of the 1923 Kanto Earthquake (Wald and Somerville, 1995)

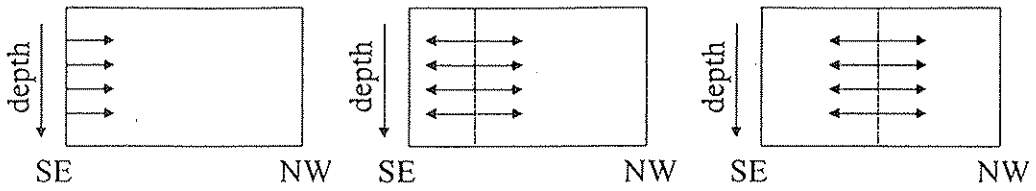

(a) Unilateral and Bilateral Rupture

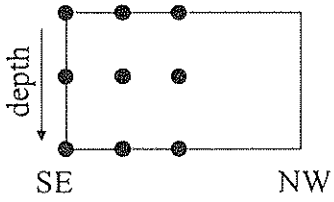

(b) Hypocenters of Radial Rupture

Figure 8 Reassigned Rupture Modes and Hypocenters of Radial Rupture

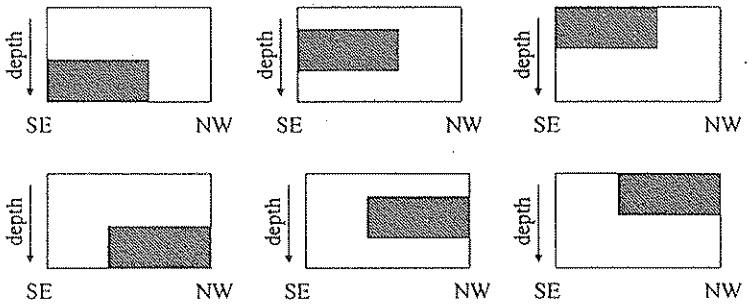

(a) 2×3 Asperity

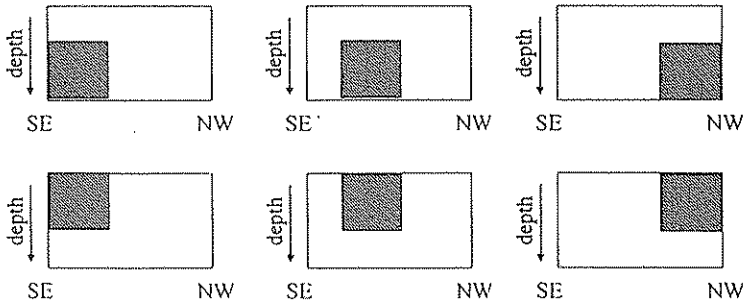

(b) 3×2 Asperity

Figure 9 Reassigned Asperity Shape and Locations

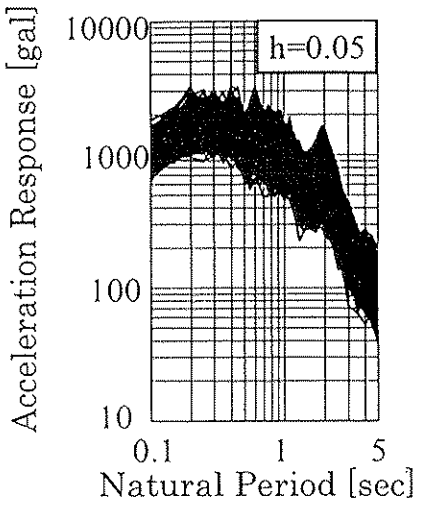

Figure 10 Acceleration Response Spectra of Synthesized Ground Motion

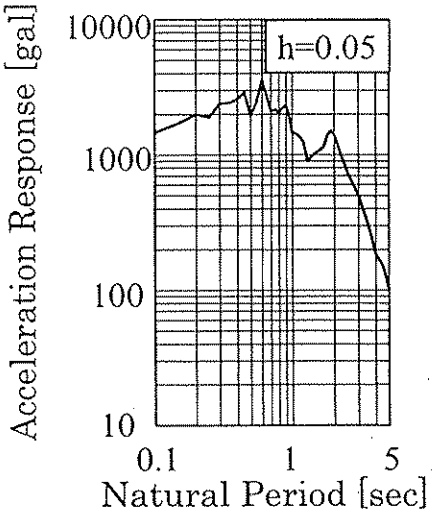

Figure 11 Acceleration Response Spectrum using the Variable-Slip Rupture Model

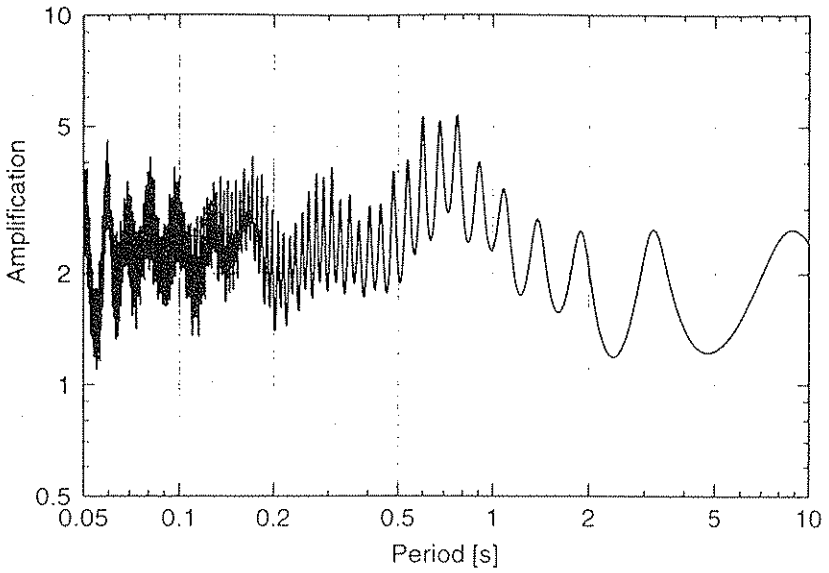

Figure 12 Transfer Function of the Ground Structure between the Ground Surface and the Seismic Bedrock at Kannonzaki

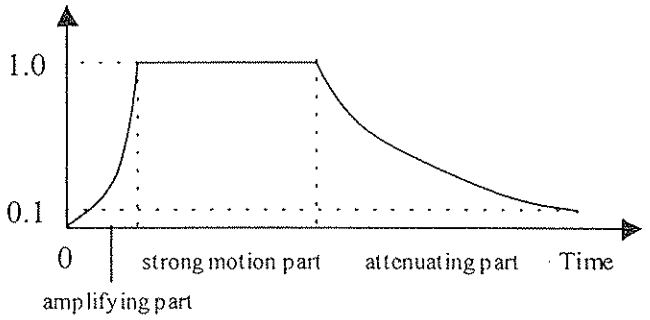

Figure 13 Shaping Window (Jennings et al., 1968)

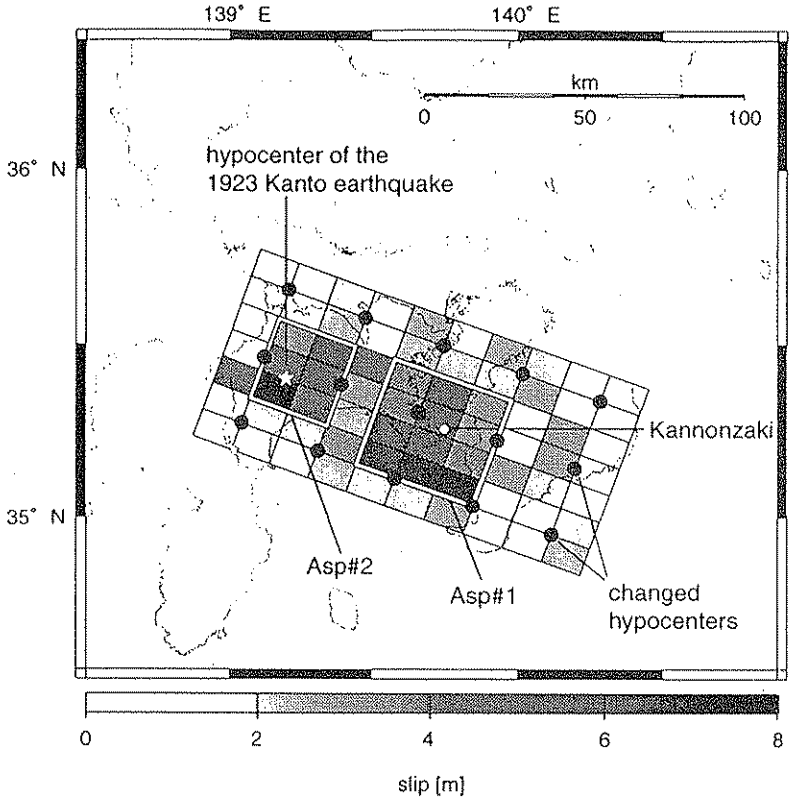

Figure 14 Rectangle Asperities Identified from the Variable-Slip Model of the 1923 Kanto Earthquake and the Locations of Hypocenters used in the Simulation

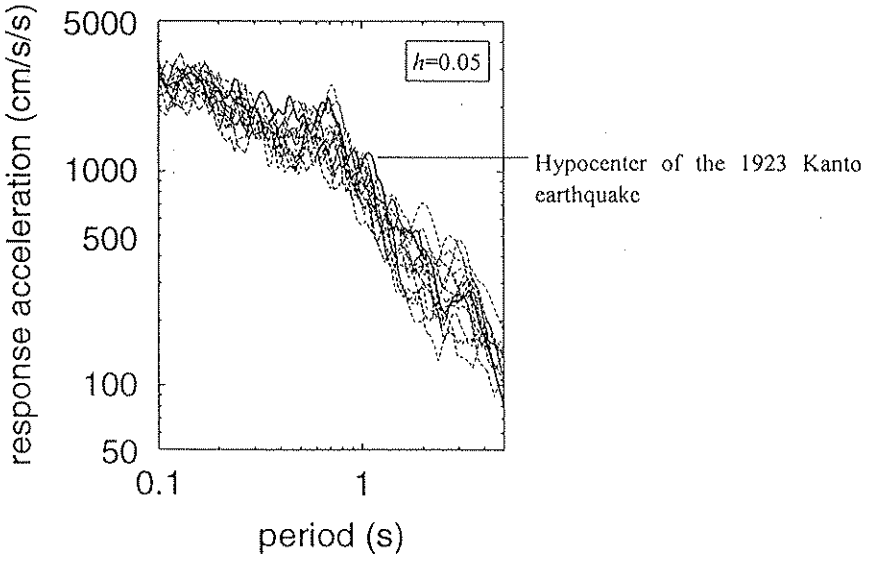

Figure 15 Variation of Ground Motion due to Location of Hypocenter

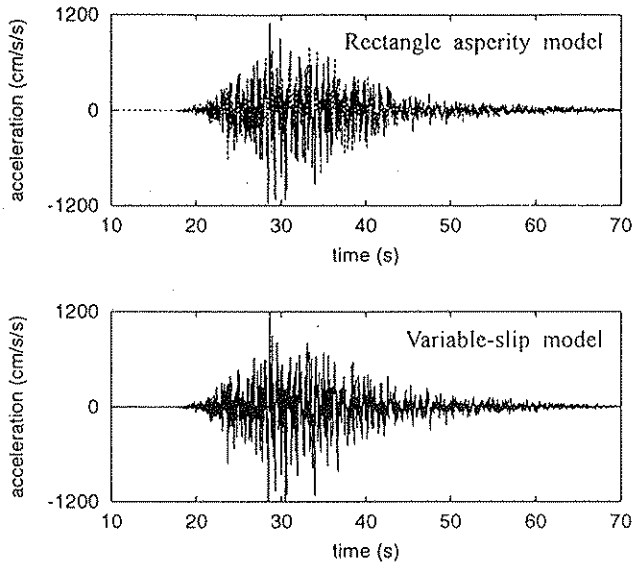

(a) Waveforms

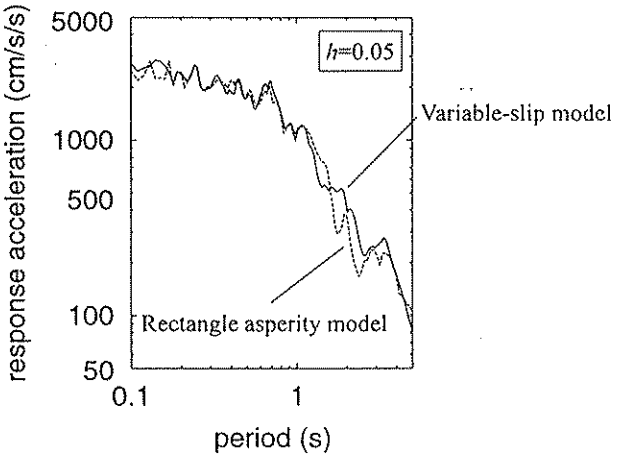

(b) Acceleration Response Spectra

Figure 16 Comparison between the Simulated Ground Motions due to the Rectangle Asperity and Variable-slip Models

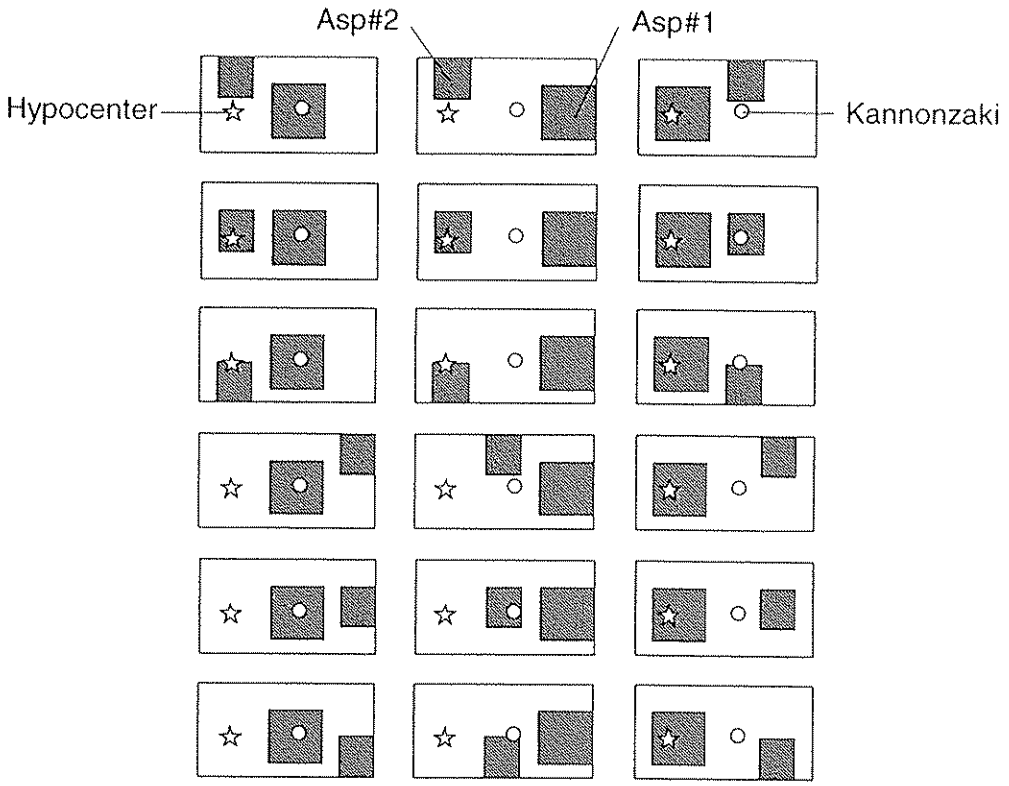

Figure 17 Rectangular Asperity Models with Variety of Locations of Asp#1 and Asp#2 The locations of hypocenter and Kannonzaki are also shown.

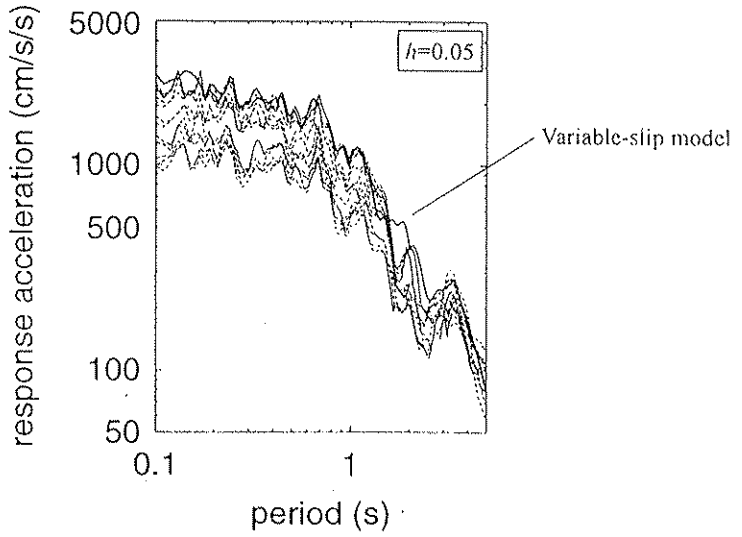

Figure 18 Variation of Ground Motion due to Location of Asperities